

FINAL

03-2377

Transmitters and Receivers in Free Space Optical Communications For Deep Space Links

“Current Areas of Research”

Jason Beebe

Jet Propulsion Laboratory

Free space optical communication has significant advantages over more conventional radio for high data-rate operations in a deep space communication network. With the support of NASA's Mars program, the Optical Communications Group at the Jet Propulsion Lab plans to put a Mars-Earth optical communication link into effect by August 2010. Two of the many research areas integral in making this a reality are optical antenna design and laser transmitter design. This paper addresses areas of both of these by exploring a mode-matched design for a cavity-dumped communication laser, and by reporting on the initial stages of the analysis of an existing 100inch telescope for use as an optical communications receiver.

The Research in this publication was carried out by the Jet Propulsion Laboratory, California Institute of Technology, under a contract with the National Aeronautics Space Administration.

I declare that this work has been composed by me, and is a record of work done by me, and has not previously been presented for a higher degree. This project was conducted by me at The Jet Propulsion Laboratory from June 19th, 2003 to August 29, 2003 towards the degree of MSc in Photonics and Optoelectronic Devices at the University of St. Andrews under the supervision of Hamid Hemmati.

Contents

	Page
I. Introduction	3
II. Project and Report Structure	3
III. Mode-Matched Design for a Cavity-Dumped Communication Laser	4
a. Discussion of a Cavity-Dumped Communication Laser	4
b. <i>Existing Laser Cavity Design</i>	5
c. Definition of Mode-Matching the Laser	5
d. Constraints Placed on the Mode-Matched Design	6
e. Formulation of the Design Plan	8
f. Results of Design Calculations	8
g. Suggested Design	10
h. Suggestions for Future Work	11
IV. Characterization of the 100-inch Telescope at Mt. Wilson Observatory for Use as a Free Space Optical Communications Ground Receiver	11
a. List of Major Parts Used in the Experiment	12
b. Experiment Plan	12
c. The Point Spread Function's Roll in Telescope Characterization	15
d. Characterization of the Telescope's Tracking Ability	16
e. Characterization of the Telescope's Blind Pointing Accuracy	18
V. Summary	20
VI. Acknowledgments	20
VII. References	21
VIII. Appendices	23

Introduction

Free Space Optical Communications is a new technology, and although there are several companies currently producing systems for ground based commercial use, deep space optical communications remains a controversial topic. Radio has had such a stronghold on space communications that the huge infrastructure surrounding it makes it hard for a new technology to break into the field. Many opponents will say that radio works fine, so why change it. And this is a large reason why a lot of the free space optical communication technology currently coming to fruition has been around only in the form of ideas and on paper for close to 30 years. Though recently there has been a new spark of interest. This has come mainly from the NASA Mars program, which has been a major driving force in the push for deep space optical communication.

The data rate demands for the retrieval of information from current space probes and crafts is higher than ever. The use of high data rate optical fiber communication links on earth has given the scientific community a taste for the transmission capabilities that only optical frequencies can provide. New high-resolution instruments for remote sensing technology and *in-situ* experimentation, small powerful computers, and smaller budgets with the demand for more efficient space missions are revealing radio as an information-transmission bottleneck and giving people reasons to believe that optical communications (with its lighter more efficient and higher bandwidth systems) is a good idea for our near-future Mars missions, as well as, though with somewhat less finely focused goals, all future space missions.

- For a good background into Free Space Optical Communications see Reference 1
- For a good background into Free Space Optical Communications at JPL see the publications at: <http://lasers.jpl.nasa.gov/PAGES/pubs.html>. A list of research topics addressed in these publications is shown in *Appendix D*.

Structure of Project and Report

The structure of this report is much like the structure of the project. There was no specific project definition but instead the assignment of several different tasks related to the design of laser communication transmitters and ground based optical communication receivers. So the report focuses on two different areas related to the tasks that were assigned.

The first task of coming up with a mode-matched design for an existing cavity-dumped communication laser was done entirely in theory. The laser that the design was for is currently being used for other purposes so implementation and testing of the design has yet to be performed.

The second task of assisting in the characterization of the 100-inch telescope located at Mt. Wilson Observatory involved a lot of acquisition and organization of equipment, as well as several late nights observing. I was provided with the experiment plan given below and, with a lot of help from primarily one other engineer and avid armature astronomer, I was given the task to complete step one of phase one (below) before my project was completed. Basically I was the eyes, ears, and hands for the author of the experiment. I performed manual tasks such as crawling around on the telescope to install temperature sensors, and technical tasks such as assisting in devising plans to test tracking and blind pointing accuracy, as well as photonics related tasks such as acquiring suitable point spread functions.

There was a third task that was written up, but that could not be released due to patent reasons.

There also were other small tasks performed related to ordering parts for and setting up a photo-spectrometer, but these tasks were minor and not included in this report. I will continue with the above projects until the middle of September 2003 and I hope to provide updates during my oral presentation given at that time.

Mode-Matched Design for a Cavity-Dumped Communication Laser

A simple inexpensive prototype cavity-dumped laser is currently being developed at JPL with the intention of demonstrating the ability of a cavity-dumped design to out perform more conventional Q-switched designs in providing high-rate operations in pulse position modulation (PPM) communications [2]. In this section we look at how a specific laser (already assembled) can be mode matched for more efficient pumping. Limitations such as using existing components or easily acquired commercial components are taken into account to produce a functional and realizable design.

Cavity-Dumped Communication Lasers *

Optical communications experiments from space are demonstrating very significant payoffs in data rates and efficiency. The European Space Agency (ESA) Advanced Relay and Technology Mission (Artemis) link has demonstrated a stable 50 Mb/s link from low Earth orbit (LOE) to geosynchronous Earth orbit (GEO) [3,4]. The goal of the JPL Optical Communications Group is to develop the technology that will allow those high data rates to be realized, and to enable the next generation of interplanetary probes to make full use of the high-resolution instruments in development.

To achieve this goal, laser technology is being developed that can support 10 to 100 Mb/s data transmission rates at deep-space [>1 astronomical unit (AU)] ranges. While a modulated diode laser is adequate for communication in the near-Earth region [3], the vast distances involved in interplanetary missions require lasers that are capable of emitting much more energetic pulses. To achieve the demonstration goal of 10 Mb/s from Mars, JPL's system design hypothesizes a laser that, under the most stressing conditions, emits up to 8 μJ per pulse at average rates of 1.5×10^6 per sec., with variable pulse-to-pulse spacing to encode the data in an energy efficient pulse position modulation (PPM) format. This must be done with materials and components that are suitable for long space-flight missions and with technology that has a development path to relatively high electrical efficiency (>10 percent).

Much previous work has concentrated on Q-switched solid-state lasers (e.g. [5,6]) and recently on master oscillator power oscillator power amplifier (MOPA) systems (e.g. [7-11]). Both of these show promise in various applications but still face challenges in development for these particular goals. It has been hypothesized that for the high modulation rates and peak powers desired, a cavity-dumped laser is in ways more suitable as a laser source [2,12-15].

Existing Laser Cavity Design

A Simple inexpensive laboratory laser has been developed by W.T. Roberts [2] at JPL with (1) an Nd:YAG laser crystal coated for high transmission at 808 nm and high reflectance at 1064 nm on one end, and anti-reflection (AR) coated for 1064 nm on the other end, (2) a 1064 nm high-reflectance (HR) mirror, (3) a 1064-nm polarizing beam splitter, and (4) a rubidium titanyl phosphate (RTP) electro optic modulator (EOM). This equipment is set up as shown in *Figure 1*.

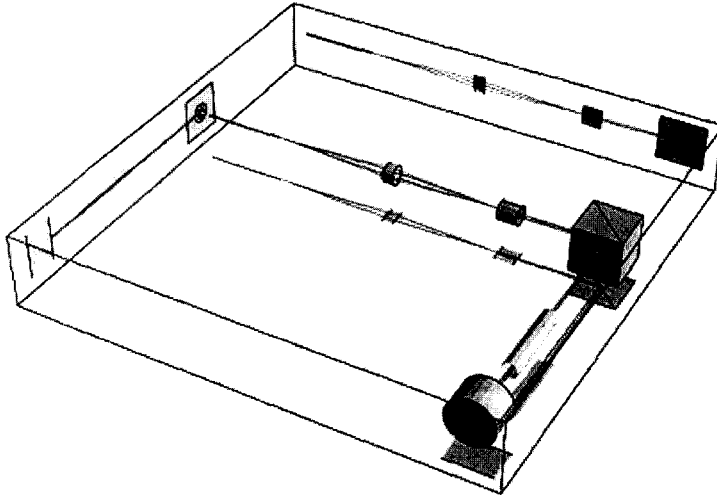


Figure 1. Optical schematic showing the laboratory design for a high-rate cavity-dumped laser. Credit W.T. Roberts

An existing 30-W fiber-coupled 808-nm (red rays) diode laser source is shown focused into the Nd:YAG laser crystal. The normal cavity oscillation mode (green rays) is shown in an L-configuration because the polarizing beam splitter is more efficient (99.9 percent) in the reflection (S-wave) than transmission. After reflecting from the internal diagonal surface of the beam splitter, the S-polarized beam then goes

through the EOM, which is normally in the off condition, and has no effect on the beam polarization. Finally, the beam reflects from the HR end mirror and retraces the cavity. When the EOM is switched on, the S-polarized wave experiences an electrically induced birefringence, changing the linearly-polarized beam to elliptical polarization, the ellipticity being dependent on the applied voltage, electro-optic coefficient of the material, and the wavelength on the beam (1064 nm). If the field is strong enough for the particular set of conditions, a quarter wave of retardation can be induced between the ordinary and extraordinary waves of the beam, creating a circular polarization. After reflection from the end mirror, the circularly polarized beam experiences the birefringence of the EOM once again, and it is changed back to a linearly polarized beam, but orthogonal to the incident polarization (P-polarized). The polarizing beam

splitter transmits P-polarized light, coupling the light out of the cavity.

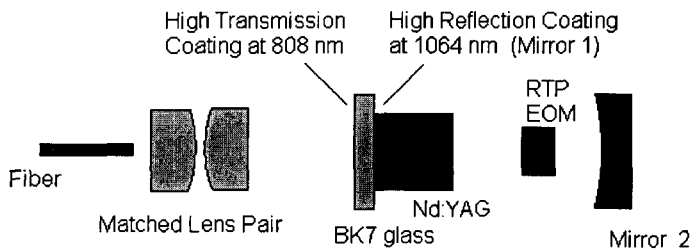


Figure 2. Conceptual drawing representing components integral to the mode-matching design.

Mode Matching

A conceptual drawing of the laser sufficient for mode-matching analysis is shown here (*Figure 2*) without the polarizing beam splitter.

In order for the circulating intracavity radiation to get the most gain out of the excited Nd:YAG crystal molecules it should overlap the most intensely pumped region of the crystal as closely as possible. As Gaussian beam optics dictates, the beam waist of the circulating radiation in a hemispherical cavity falls at the surface of the flat mirror. So in order for the radiation to best overlap, the beam waist of the focused pump light should also fall at this surface. The beam waists should also be the same size (*Figure 3*). In other words, the beams should be mode matched.

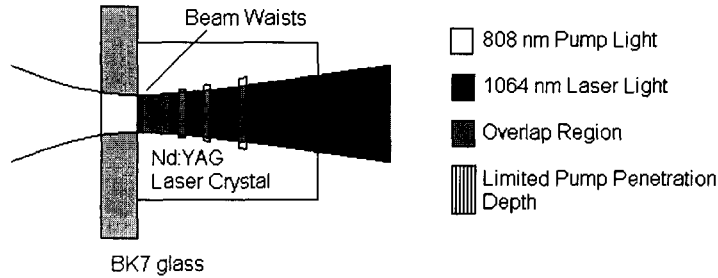


Figure 3. Two beams are mode matched when their waists are the same size and fall in the same space.

Getting the beam waists to fall at the same place is relatively simple. The matched lens pair is used to focus the pump light down to a point falling at the inner surface of the flat laser

mirror. The more complicated task is to match the beam waist sizes. The waist size of the pump light is

limited by the size of the image of the fiber core. This is because the Gaussian beam waist of the pump light is essentially the image of the fiber core. If the matched lens pair is configured to provide 1 to 1 magnification, then the beam-waist size of the pump light will be the size of the fiber-core, which is 100 microns in diameter. The beam waist of the hemispherical laser cavity depends on both the radius of curvature of the spherical mirror and the length of the cavity, and can be calculated through the following relation [19]

$$\omega^2 = (L_{op}\lambda/\pi) \times [g/(1-g)]^{0.5} \quad [1]$$

where ω is the radius of the beam waist, L_{op} is the optical cavity length, λ is the wavelength of circulating light, and g is the *g-parameter* [19] for a half-symmetric resonator;

$$g_2 = 1 - L_{op}/R_2 \quad [2]$$

where R_2 is the radius of curvature of mirror 2.

Constraints

There are several constraints placed on the geometry of the mode-matched design due to the fact that the laser had already been assembled and there was a desire to avoid any new costs

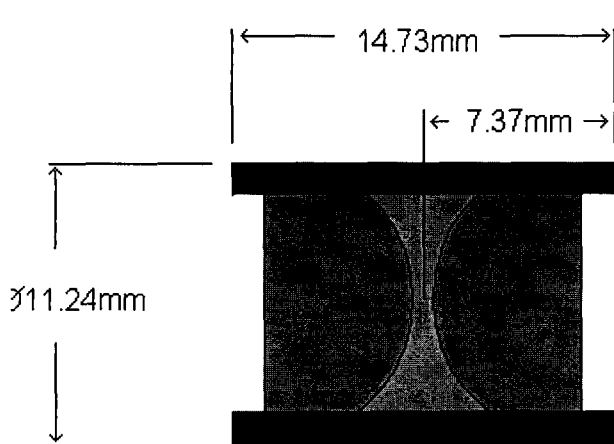
associated with the purchasing of new components. The first component important to mode matching and placing constraints on the design is

- The pump fiber.

The current pump fiber has a 100micron core diameter, d . As noted above, this plays a roll in the size of the pump light beam waist. The second component important to mode matching and placing constraints on the design is

- The matched lens pair used to couple the pump light into the laser.

This matched pair can be considered to be a thick lens with an effective focal length of 11.0mm. The lens was chosen for its large numerical aperture (NA) of 0.25 and is shown in *Figure 4*



This lens not only places constraints on the design do to its focal length and NA, but also do to the geometry of the housing which limits how close the lens can be placed to the laser. The third component important to mode matching and placing constraints on the design is

- The 1/8th inch thick plate of BK7 glass.

Figure 4. Schematic of matched lens pair used to couple the pump light into the laser.

This component is important because it limits how close the matched lens pair can be place to the beam waist

location of the laser light and also because the pump light being focused into the cavity refracts through the BK7 glass. This refraction serves to lengthen the focal length of the lens pair by a small amount, which may be important in determining the location of the pump-light beam-waist. The fourth and fifth components important to mode matching and placing constraints on the design are

- The Nd:YAG and RTP crystals.

The length and refractive index of these components are important because they affect the optical length, L_{OP} , of the cavity. This will affect where mirror 2 should be placed in order to get a specific laser beam waist size. The sixth component important to mode matching and placing constraints on the design is

- Mirror 2.

The radius of curvature of mirror 2 affects the size of the circulating radiation's beam waist. The radiuses of curvature allowed in the design are those that readily available commercial laser mirrors come with. For example: 0.5m, 0.75m, 1.0m etc.

The final constraint placed on the mode-matching design is the desire to have a 3 or 5 nanosecond cavity round-trip time, τ_{RT} . This shortens the cavity length and facilitates easier alignment.

Design Plan

The design plan was as follows.

1. Find the optical cavity lengths for the desired round trip times.
2. Pick a standard radius of curvature, R, for mirror 2 that is close to this size (close to L_{op}).

We know that, for beam waists of about 100 microns, that R must be approximately equal to L_{op} from analysis of the following equation [19]:

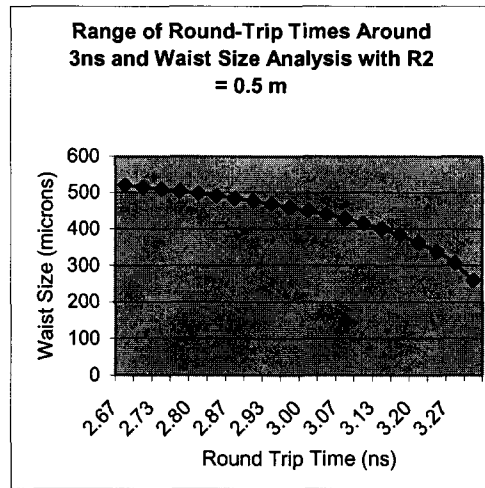
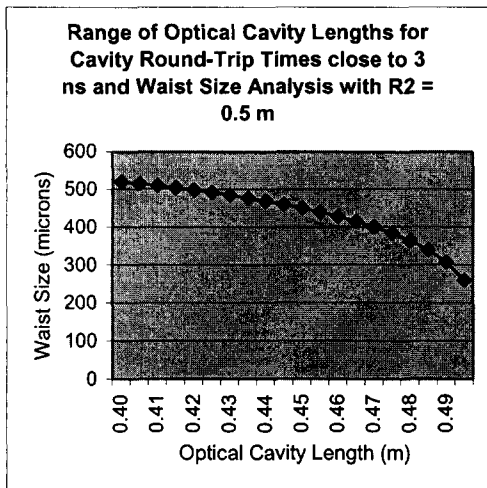
$$\omega^2 \approx L_{op} \lambda / \pi * [L / L_{op}]^{0.5} \quad [3]$$

Where $R = L_{op} + L$.

3. Calculate beam waist diameters for these L_{op} and R values using Equation 1.
4. Determine the cavity lengths, L, that will give these L_{op} values from the length and index of refraction values of the Nd:YAG and RTP crystals.
5. Determine the geometries of the external-cavity optics based on the magnification of the fiber core that is required to match these beam waist sizes at the inner surface of the flat laser mirror, and based on the shift in the focus of the lens pair due to the BK7 glass plate.
6. Pick the geometry that makes the most sense. Meaning, pick the design where the distances between components aren't so long or so short that assembly is not feasible or impossible, and where the lens pair focuses all of the pump-light into the laser. If all geometries provide this then pick the design that will be easiest to assemble or the one requiring a mirror 2 that will be easiest or cheapest to acquire.
7. If the design is not feasible, relax some of the constraints.

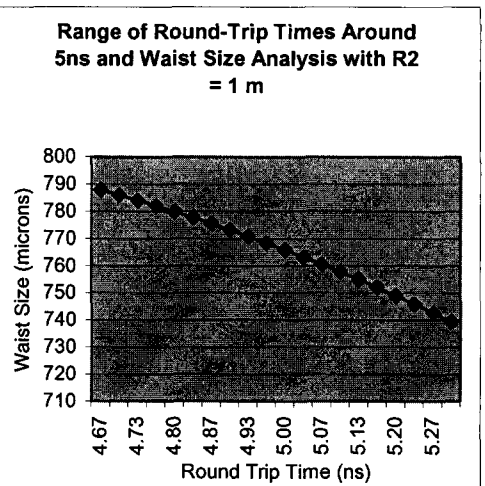
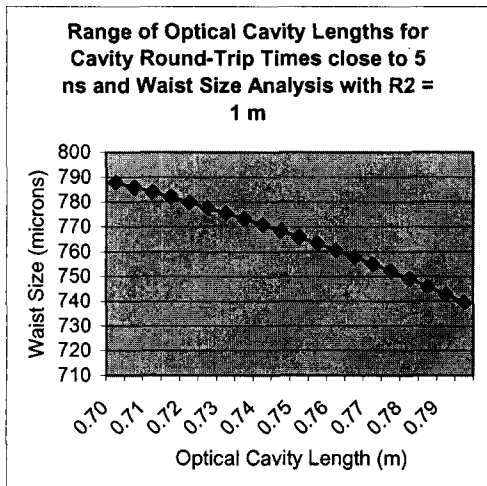
Results of Calculations

A range of waist sizes for the round trip-times close to the desired 3- and 5-ns times and for the corresponding cavity optical lengths are shown in *Figure 5*.



(a)

(b)



(c)

(d)

Figure 5 a,b,c,d. A range of waist sizes for the round trip-times close to the desired 3- and 5-ns times and for the corresponding cavity optical lengths.

Because we know that the fiber core is 100 microns, these plots also tell us what magnification (M) is needed to match the pump beam waist size to the laser resonator waist size. *Figure 6* shows what distance (u) the fiber would have to be placed from the center of the lens pair to achieve the magnifications required for matching the waist sizes in *Figure 5*.

These distances (u 's) were determined using the lens equation

$$1/f = 1/u + 1/v$$

[4]

where $f = 11$ mm and where v is the distance from the center of the lens to the image (i.e. to the inner surface of mirror 1) and is equal, from geometric optics, to $M \cdot u$. And the M values were

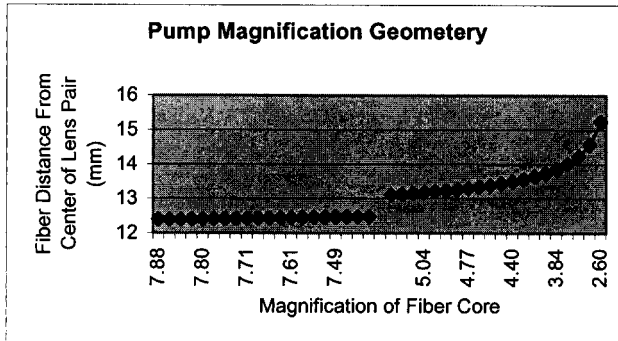


Figure 6. A Plot showing how far the fiber should be placed from the center of the lens pair to get the particular magnifications of interest for ranges of cavity times around 3 and 5ns.

determined by dividing the laser waist sizes in *Figure 5* by 100 microns (the size of the fiber core). And in turn we can see how far (excluding the shift due to the refraction through the glass of mirror 1) the center of the lens pair should be placed from the inside surface of mirror 1, namely that distance is $M \cdot u$.

To determine the cavity length (L) we consider the optical length of the Nd:YAG crystal and of the RTP crystal. The refractive index (n) of Nd:YAG is 1.82 making the optical length ($n \cdot L$) of the 5mm long crystal 9.1 mm. The refractive index of RTP is 1.9, making the optical length of the 20 mm long

crystal 38 mm. Because of this, the actual length (L) of the cavity should be shorter than the chosen optical length (L_{op}) by 22 (9.1-5 + 38-20) mm.

Suggested Design

A design having a cavity round trip time close to 3 ns is suggested due to the smaller cavity length and also due to the shorter distances needed between external cavity optics in order to get

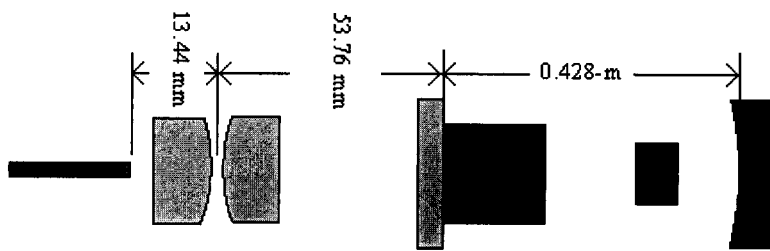


Figure 7. Suggested placement of optics.

requires u to be equal to 13.44 mm and v to be equal to 53.76 mm. See *Figure 7* and *Figure 8* (figures not to scale).

Again this is only a suggestion. The plots in *Figures 5* and *6* can be used as a guide in getting a feeling for the size and geometry of a mode matched design for this particular laser. The method itself can serve as a guide in mode-matching a fiber-pumped hemispherical laser cavity in general.

the required magnification. Choosing the 3 ns cavity will give a cavity length of 0.428-m, a beam waist size of 450.79-microns requiring a

pump light magnification of 4.5079 which

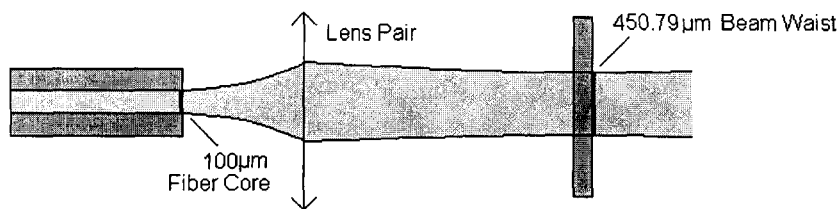


Figure 8. Diagram indicating the roll of the lens pair in matching the pump waist size to the laser waist size.

Suggestions for Future Work

This design did not take into account the shift in the focal point of the pump light due to refraction through the 1/8" BK7 glass plate. This shift should be small and should not effect the efficiency of mode-matching that much. But this shift would probably want to be taken into account before any serious applications of this design.

In the calculations to determine magnification and lens placement the lens equation was used which assumes a "thin lens." The matched pair is relatively thick compared to its focal length and it is possible that it acts more as a "thick lens." If the later is the case, a more thorough ray tracing approach should possibly be taken.

It was also not verified that the numerical aperture (NA) of the lens pair is large enough to accept all of the pump light from the fiber. This should also be verified.

Whereas this portion of the paper has been dedicated to a more theoretical side to Deep Space Wireless Optical Communications the next portion moves to "the other end" both figuratively and literally speaking as we shift our focus from theory to experimentation and from transmitting to receiving.

Characterization of the 100-inch Telescope at Mt. Wilson Observatory for Use as a Free Space Optical Communications Ground Receiver

The ground station for deep-space optical communications is a unique instrument [16]. Several characteristics set apart a free space optical communications telescope receiver from a traditional optical telescope. Most notably, it has no imaging requirements, but must effectively focus incident photons onto a detector of relatively large but finite diameter. The ground station must also operate at very small Sun-Earth-probe angles in order to minimize communication outages.

However, while operating near the Sun, the ground station must not lose sensitivity to the incoming spacecraft signal due to stray sunlight impinging on the detector, or due to thermal stresses on the receiver structure. The requirement that the ground station have excellent stray-light rejection characteristics is one that is common with high-quality astronomical telescopes [17]. Actually, the ground station and high-quality astronomical telescopes have many things in common.

So the question being posed is: can existing optical telescopes be used as deep space optical communications ground receivers? To begin answering this question the Optical Communications Group at JPL has started an experiment to characterize the almost 90- year old 100-inch (primary mirror) astronomical telescope located at Mt. Wilson Observatory overlooking Los Angeles from the San Gabriel Mountains. In this section of the paper this experiment is discussed and some initial results are presented.

Parts

Telescope

- A blueprint of the telescope being characterized including a superposition of the actual position of the current optics is shown in *Appendix A*. A picture of the telescope is shown in *Appendix B*.

Camera

- A scientific grade Apogee AP47p CCD was installed at the Cassegrain focus of the telescope and plays an important role in characterization.

High-Rate Detectors

- Various photon-counting detectors will replace the camera at the telescope focus for a second phase of the experiment.

Temperature Sensors

- Temperature sensors were installed at various locations on the telescope. A schematic showing the placement of the temperature sensors is shown in *Appendix C*.

Experiment Plan **

This experiment is currently in the first phase of a two-phase experiment. The first phase involves characterizing the telescope during normal nighttime operation and then again in the presence of heating due to daytime use. The characterization consists of analyzing the telescope's point spread function (PSF), blind pointing accuracy, and tracking accuracy before and after heating. Temperature sensors installed before the start of phase-one will monitor telescope temperature throughout the experiment. The second phase of the experiment at Mt. Wilson is more of a technology demonstration. This phase will incorporate the use of photon-counting detectors at the telescope focus. The detectors used will be the kind of detectors that will be used in deep space optical communication links. The demonstration will compare different detector candidates and provide valuable information for use in designing the receiver-

terminal tracking system, and provide experience in using photon-counting devices for high-bandwidth measurements in a receiver-terminal environment.

Phase One

1. An Apogee Ap47p CCD camera was installed at the Cassegrain focus of the telescope (see *Appendix A*), using a standard 21-inch telescope mounting plate. The camera was placed at the nominal telescope focal point and optimized for the best centration and focus of the image of a star near zenith pointing. The experiment was started early August 2003 and the goal was to have measured the point spread function of the telescope, blind pointing accuracy, and tracking accuracy of the telescope over the full range of right ascension (RA) and declination (Dec) available on the telescope before the end of August 2003. A total of at least 20 bright stars will have been measured at varying locations in RA and Dec. The point spread function data will be used to evaluate telescope optics alignment and centration under varying gravitational sag, and be used as a basis for comparison with such measurements after the telescope has been thermally stressed. The pointing accuracy and tracking accuracy at varying locations in RA and Dec will provide information for determination of open-loop track parameters for ground receiver pointing.
2. After completion of the preceding plans, thermal stress will be introduced to the telescope structure and mount. The initial stress will be introduced by opening the telescope dome and operating the telescope during daylight hours, for a continuous 12-hour period. Shortly after sunrise, the dome will be opened and images of bright stars will be taken. For these initial tests, no portion of the telescope structure will be directly illuminated by sunlight. The temperature at various points on the telescope structure and mirrors (see *Appendix C*) will be continuously monitored throughout the experiment, and has been monitored since before the first star pictures were taken. At 3-4 times throughout the night, stellar point spread functions will be measured at various sky locations. The results will be compared with the previous PSF measurements to observe the effects of heating the dome. These measurements will be continued for a period of 3 consecutive days to allow a buildup of dome heat. The data will be analyzed to determine performance of the telescope under thermal stresses introduced by heat accumulation in the telescope dome. In addition, sky background measurements will be used in calibrating with simultaneous Aeronet [18] measurements. Finally, dome recovery time from various elevated temperatures will be obtained.
3. The final set of measurements to be obtained in the first phase of the plan will be concentrated on measurements of telescope performance while gradually introducing the telescope to increasing thermal stresses. The telescope will be gradually pointed closer and closer to the sun, noting the portions of the telescope that are directly illuminated by sunlight, and approximate duration of such illumination. Similar measurements of point spread functions during daylight hours will be made on stars as the telescope is pointed gradually closer to the sun. During the first day, we expect to get within 35 degrees of the sun, within 15 degrees on the second day, and as close as possible on the third day (calculations indicate that we should be able to get within 10 degrees). In no case will the sun be allowed to directly illuminate the telescope primary mirror. At the completion of these measurements, periodic nightly stellar images will be obtained until the telescope has relaxed to its nominal operating conditions. The point-spread functions obtained will

be compared with the previous values to determine the magnitude and type of aberrations in the telescope induced by heating of the support structure. Background data will be used for calibrating near-sun-*in-situ* sky radiance measurements. Telescope relaxation times from thermal stresses will also be determined.

Phase Two

1. In this phase of the experiment an assembly will be placed at the Cassegrain focus of the 100-inch telescope that will allow for data to be taken with photon counting avalanche photodiode (APD) detectors currently in development in the laboratory. The instrumentation is expected to use both the Apogee camera from the first phase of the experiment, and the APD's, either directly placed at the focus, or fiber coupled to the focal point. A removable beam-splitter will be used to switch between devices. The setup will require mounting the instrument, optimizing the position of the Apogee camera for centration and focus, and co-registration of location of the APD or its fiber feed.
2. Photon-counting operation will be demonstrated by observing a very dim star on the APD. Pulsars and bursters may likewise be observed.
3. Measurement of the narrow-band Mars background light will be obtained by incorporating an existing 1 Angstrom NIR (1020 nm) filter.
4. Long- term measurements of a star will be obtained on the APD detector in open loop tracking to establish requirements for the fine-steering mirror to be used in future tracking experiments.
5. Measurement of sky background light will be observed through the narrow-band filter. This data will be correlated with simultaneous *in-situ* measurements with the Aeronet spectral radiance system.
6. Data will be taken with the following detectors which range from commercial to commercial-custom hybrids to custom, and then later analyzed as part of the detector selection process:
 - a. A Si APD with high gain on the order of 1000. A cryostat setup will be used in order to keep the detector temperature at 270-K and the amplifier at 77-K.
 - b. A photon counting detector of either Ge or As doped Si with both detector and amplifier kept at a temperature of 10-K.
 - c. A Geiger mode detector made of either Si or In:GaAs.

In this paper the theory and data of step one of phase one will be addressed. About 100 images of stars have been taken so far and at least one test for blind pointing accuracy and one test demonstrating tracking accuracy has been run. This paper will show that separating the distortion effects in an image due to the atmosphere and those due to the telescope aberrations is a complicated task possibly requiring the superposition of many images. Determining the distortion effects due to the atmosphere-telescope system as whole, on the other hand, is a relatively simple task that requires little more than simply taking a picture of a star. The blind

pointing accuracy test that was run provides some rough quantitative data as to how well the telescope can point to a specific parts of the sky simply given the coordinates. And the tracking accuracy test shows that the telescope's current tracking capabilities are well below those that would be required for a free spaces optical comm. receiver. Though the tracking data, pending some information about the telescope's drive mechanics, should be able to put us on the right path towards developing a correction.

The Point Spread Function

No image is a perfect representation of the real world. All images have noise in them caused by the detection process. All images are also blurred to some extent; whether by focus problems, fundamental limitations or errors in the optics, motion blur, or the effects of air currents in the atmosphere. All of these blurring effects can be modeled by a single Point-Spread Function (PSF). Mathematically speaking the PSF is convolved with the original (perfect) image to produce the (blurred) picture at the detector.

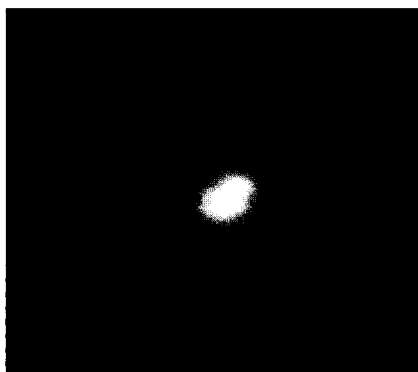


Figure 9. The intensity profile of an image of a star is the PSF describing all of the distortions affecting the light.

Let's assume a photograph is taken of something that is known to be a perfect point of light. An example of this would be a star image – aside from the Sun, stars are much too far away from the Earth to be resolved by conventional optical systems. The actual image on the

photograph would not be a perfect point like the real star because of various blurring effects. The intensity

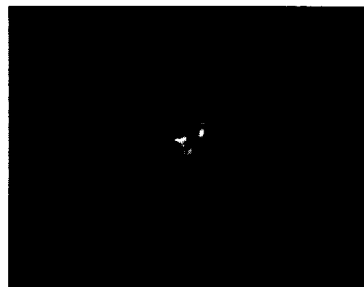


Figure 10. A short exposure allows you to see the speckles due to scintillation of the atmosphere.

profile of the blur in the picture is actually itself an accurate measurement of the PSF which blurred the image. An example of a star image, and therefore a PSF, taken through the Mt. Wilson 100 inch telescope is shown in *Figure 9*. The PSF due to scintillation of the atmosphere will usually show up as a Gaussian, where as the PSF due to telescope aberrations can usually be described as an exponential. The image in *Figure 9* is a 12 second exposure taken through a neutral density filter of optical density 2. Sometimes a shorter exposure, such as that in *Figure 10*, gives a better idea of exactly how the atmosphere is affecting the light. The image in *Figure 10* was taken with no neutral density filter at an exposure of one millisecond. The light moves around on the CCD because of varying temperature, and therefore varying index of refraction, air masses in the atmosphere moving above the telescope. These air masses cause the wave fronts of the star to refract, or twinkle. In the absence of scintillation the star image in *Figure 10* would be a single dot (with some telescope introduced aberrations) at the center of where a speckle pattern can now be seen. The light is less and less likely to refract further away from the speckle pattern resulting in the Gaussian distribution. Over a longer exposure such as that in *Figure 9*, the speckles blend together and you get a smooth Gaussian. This Gaussian smoothing of sharp points can also be seen in the blurring of the surface features and border of the Mars image in *Figure 11*. An image of Mars taken with the 100-inch telescope should have

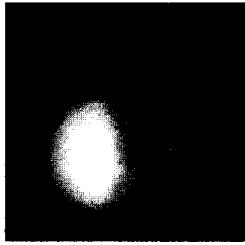


Figure 11. An image of Mars demonstrates the application of the PSF to every point in an image.

been much clearer (especially on that night when Mars was closer to Earth than it has been, within a few days, in 57,000 years). The PSF described by the star image is applied to every point in the image.

In the longer exposure star images that were taken a nice Gaussian pattern was not seen. This is due to several factors. One, the neutral density filter may be causing some blurring due to the “speed” (about $f/16.6$) of the telescope and reflections off of the inner filter surfaces (Figure 12). Two, faults in the tracking system (see below) begin to show themselves during long exposures. This can be seen in how the image in Figure 9 is somewhat smeared across the CCD (Figure 13). Three, telescope

aberrations are also buried in this image somewhere. One idea for how to extract them is to take many short exposure images such as those in

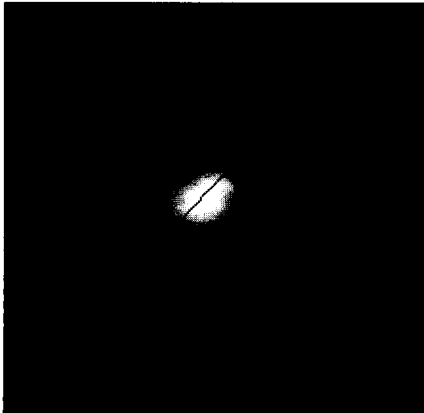


Figure 13. The line shows the direction in which the image is smeared due to tracking errors.

Figure 10, and sum them in a fashion such that you only add the parts that are alike. This should get rid of much of the speckle. Also using short exposures and no filters will avoid distortions like those in Figure 12.

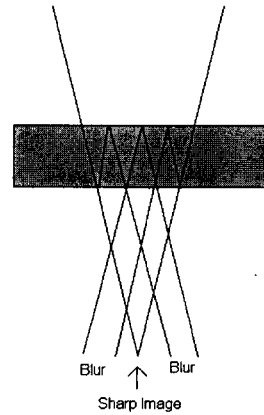


Figure 12. To avoid blurring due to any filters, this light passing through a filter should be as collimated as possible.

PSF Conclusions

Over 100 images have been taken over all parts of the sky. These images themselves serve as point spread functions to be used for comparison in later parts of the experiment. To determine exactly how the thermal stress are affecting the telescope it would be necessary to separate the atmospheric and telescope distortion PSF’s from all of the images.

Tracking

To maintain a communication link with a spacecraft the ground receiver has to be able to track the spacecraft as it moves through space. The 100-inch telescope is equipped with its own tracking system. And it is this tracking system as a whole, including any hardware or software, that this section addresses the current performance of. The goal is to determine just what type of correction the current tracking system will need in order to meet optical comm. ground receiver requirements.

One simple test was run to observe tracking. A star was imaged with an exposure of 500 seconds (about 8 minutes) and the pattern on the CCD was observed (*Figure 14*). There are three different types of tracking errors that are evident in *Figure 14*.

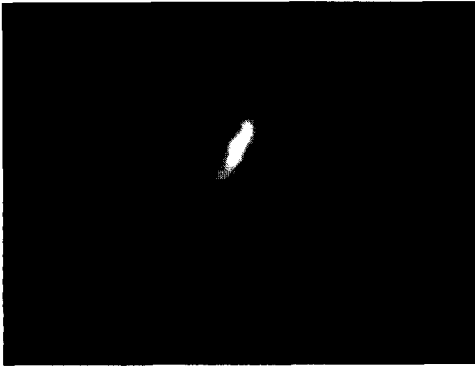


Figure 14. Without tracking errors this image should be a single Gaussian intensity pattern.

1. Polar Alignment Error

As the Earth rotates on its axis the sky appears to move around the Earth on that same axis. And far away objects in space, such as stars appear to move around this axis. If the telescope's polar axis is not parallel with the Earth's axis the telescope will track along a slightly different path than the star's motion. This error will show up in an image as a drift north or south. North in *Figure 14* is to the left. And we can see that because the image drifts north that there is a polar alignment error. If the image did not trail off the CCD before the end of the exposure then we would have had a time reference and the amount of drift could have been quantified, because we know the number of arc-seconds per pixel (about 0.06 arcsec/pixel). The drift can still be quantified, but

something else in the image that provides a reference to time must be used. What can be used is the stair-step pattern that we see as the image drifts. These steps occur once per revolution of a worm (gear-type) screw that is used to control the telescope. So if we know how many seconds are represented by each revolution of the worm screw then we can know how many seconds it took to drift a certain distance in angle north. The sec/revolution data should be on file at Mt. Wilson. This error also depends on the telescope's right ascension and declination. The farther the telescope is pointed away from zenith, the more pronounced the error would be. The reason that this stair-step pattern shows up at all is due to a second type of error known as the periodic error.

2. Periodic error

- a. Periodic error is due to inconsistent tracking rates of the telescope drive. This typically results in a back and fourth (here east and west) movement of the star image on the CCD array. This back and fourth movement should average out such that the telescope follows its target. When it does not, you have a third type of tracking error known as Average Tracking Error.

3. Average Tracking Error

- a. Described just above. This is why we see the image drift west (down) in *Figure 14*.

Tracking Test Conclusions

It appears that an auto-guider may be needed to correct for the errors in the current tracking performance. For modern auto-guiders a portion of the target's light is split off to a CCD camera that is connected to the telescope drive mechanism. The CCD tries to keep the star centered on the same pixel by providing feedback to the telescope control

mechanism. Just how much light can be spared for such a process when receiving very low power optical comm. signals from space is a topic for another discussion. In order to not use an auto guider and simply use the exact location of the target in the sky will require improvements in the telescope control.

Blind Pointing Accuracy

Giving the telescope controller the RA and Dec of a target and then letting the telescope go there without the interference of a person controlling the telescope or using some sort of finder is *blind pointing*. Just how well a telescope does this is *blind pointing accuracy*. Various factors affect the level of blind pointing accuracy, many of them being mechanical. For example in moving a large heavy telescope from zenith to a target near the horizon a tremendous amount of stress is put on the telescope structure do to it's own weight. Stress like this can move the telescope off its target. The hope is that deformations like these are repeatable and therefore that a look-up table can be created to drastically improve blind pointing accuracy. Besides the requirements for an optical comm. receiver to be able to blind point to a target, blind pointing will be required for the second part of the first phase of this experiment when stars will be acquired during the day and therefore be drowned out by background light in the operators view-scope.

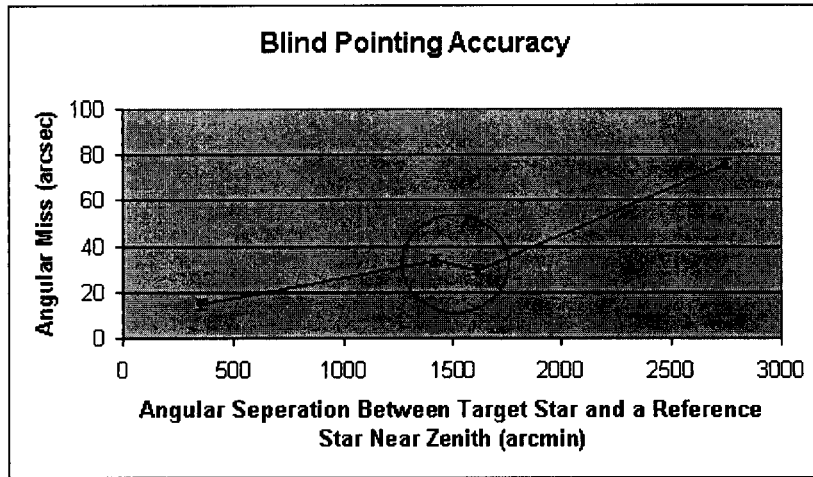
To get an idea of how well the telescope can blind point, the following procedure was followed:

1. The telescope operator uses her finder scope to center the telescope on a star near zenith.
2. Here the encoders measuring the telescope's movement are reset to that star's known RA and Dec.
3. An image of this star is taken. This image should be near the center of the CCD image.
4. The telescope operator tells the telescope to move to a star.
5. When the telescope thinks it is there, another image is taken.
6. The number of pixels between the center of the first star image and the second star image are counted. And because the direct relationship between pixels and arc-seconds has already been determined, we can determine how many arc-seconds the telescope missed its target by.
7. This is repeated for stars that are farther and farther away from zenith on the celestial sphere and in as many directions between north, south, east, and west as possible. When the target star is off the CCD, the limits of blind pointing have been reached.
8. How much it missed by can still be determined by:
 - a. Noting the RA and Dec that the telescope landed at (the coordinates that the star was told to go to).
 - b. Moving the telescope manually to center it on the target star.
 - c. Noting what the RA and Dec read now.
 - d. And by finding the angular separation between these two coordinates (those found in a. and those found in c.)

Blind Pointing Accuracy Results

Figure 15 shows the results of the blind pointing accuracy test. The accuracy of the data points in the circle is somewhat fuzzy. Because the images for these points fell right on the edge

of the CCD's field of view it was difficult to determine the exact location of their center. Because they fell right on the edge though they provide a good idea of the limitations of blind pointing



accuracy in the direction that the test was run. The target stars were generally in the south. A chart containing some data, including RA and Dec., on these target stars can be found in Appendix E. The fourth data point was well off the CCD field of view and the angular miss for it was measured as described in step 8 of the blind pointing procedure above.

Figure 15. Four stars south of zenith.

Blind Pointing Accuracy Conclusions

This was one small test for blind pointing accuracy. It provides a good feel for what the blind pointing accuracy limitations might be, but more tests in more direction with more targets should be run in order to be thorough.

Temperature Sensors

The temperature has been monitored throughout the experiment and will continue to be monitored until the end. The temperature data should play a major roll in the second part of Phase 1 when the telescope will be heated by the sun.

Summary of Mt. Wilson 100-inch Telescope Experiment Thus Far

Whether existing telescopes like the 100-inch at Mt. Wilson can be used as optical comm. receivers during the day (or even during the night) is yet to be seen. Maybe some degree of functionality serving this purpose will be found and, if they are not used as full-fledged receivers, than maybe they can be equipped to serve as a backup in case of an emergency. Determining just how useful existing telescopes will be to free space optical communications will involve more study.

Summary

It is a long road to proving the capability of Free Space Optical Communications to out perform radio for use in deep space. But with the assignment of a well-defined near-future mission and the support of NASA's Mars program, the Optical Communications Group at JPL has been able to focus its goals more tightly and are growing closer and closer to demonstrating the practicality of incorporating optical frequencies in a deep space communications network. Experiments like the ones described above have been designed to support the advancement of Free Space Optical Communications as a whole, but more specifically, have been designed to answer certain questions and overcome certain obstacles presented by the 2010 Optical Mars link mission. The hope of the Optical Communications Group at JPL is that belief in the technology such as this will finally provide the support needed and allow for the chance to prove the great capabilities of Free Space Optical Communications for use in Deep Space.

The Research in this publication was carried out by the Jet Propulsion Laboratory, California Institute of Technology, under a contract with the National Aeronautics Space Administration.

Acknowledgments

I would like to thank Jeffrey Charles for his expertise and guidance in all areas of astronomy, for working late nights, and for doing much of the work that made doing the Mt. Wilson portion of this summer project possible for me. I would like to thank him for allowing me to use his photographs and schematics (Appendix A, B, and C), and for answering my questions about and editing my section on tracking errors.

I would like to thank Tom Roberts for allowing me to work with him this summer and for finding me projects that would help me meet the requirement for my MSc degree. I would also like to acknowledge all of Tom's previous work in Cavity-Dumped Lasers [i.e. 2], and for devising such an interesting experiment for the 100-inch Mt. Wilson telescope.

I would like to thank Hamid Hemmati for supervising me this summer and for allowing me the freedom to pick projects that I was interested in.

I would like to thank Bruce Sinclair and Ajoy Kar for their support and organization of the MSc course. And Bruce specifically for helping me to coordinate doing my project back home in the states, and for allowing me the freedom to choose to do my oral presentation by video link if I wish.

I would like to thank Ian Ferguson for giving me the opportunity to participate in this MSc program at all, and for giving me the opportunity to spend 10 beautiful months in Scotland.

I would like to thank Bill Liu for letting me live in his living room this summer.

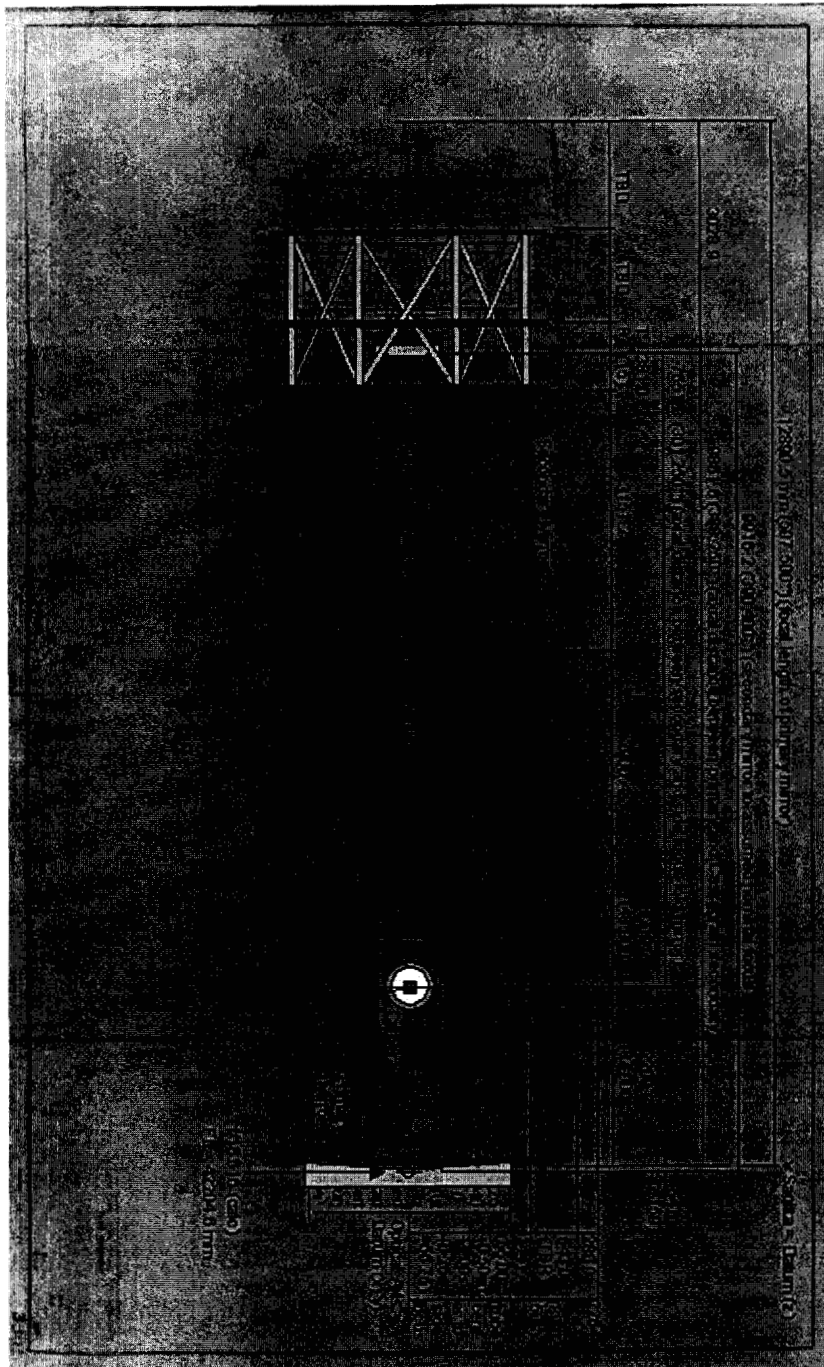
And most importantly I would like to thank my family: Mom, Tom/Dad, and Michael, and my girlfriend, Ellen, for putting up with me being away from home for so long.

References

- [1] Dennis Killinger, "Free Space Optics for Laser Communication Through the Air," *Optics and Photonics News*, The Magazine of The Optical Society of America, pp. 36-42, October 2002
- [2] W.T. Roberts, "Cavity-Dumped Communication Laser Design," IPN Progress Report 42-152, Jet Propulsion Laboratory, Pasadena, California, February 15, 2003
- [3] T. Tolken-Nielsen and G. Openhauser, "In-Orbit Test Results of an Operational Optical Intersatellite Link between ARTEMIS and SPOT4 SILEX," *Proceedings of the SPIE*, vol. 4635, pp. 1-15, January 2002.
- [4] M. Reyes, Z. Sodnik, P. Lopez, A. Alonso, T. Viera, and G. Oppenhauser, "Preliminary Results of the In-Orbit Test of ARTEMIS with the Optical Ground Station," *Proceedings of the SPIE*, vol. 4635, pp. 38-49, January 2002.
- [5] W.K. Marshall, K. Cowles, and H. Hemmati, "Performance of Efficient q-Switched Diode-Laser-Pumped Nd:YAG and Ho:YLF Lasers for Space Applications," The Telecommunications and Data Acquisition Progress Report 42-95, July-September 1988, Jet Propulsion Laboratory, Pasadena, California, pp. 168-173, November 15, 1988. http://tmo.jpl.nasa.gov/tmo/progress_report/42-95/95P.PDF
- [6] H. Plaessmann, K.S. Yamada, C.E. Rich, W.M. Grossman, "Subnanosecond Pulse Generation from Diode-Pumped Acousto-Optically Q-Switched Solid-State Lasers," *Applied Optics*, vol. 32, no. 33, pp. 6616-6619, November 20, 1993.
- [7] H. Plaessmann, S.A. Re, J.J. Alonis, D.L. Vecht, and W.M. Grossman, "Multipass Diode-Pumped Solid-State Optical Amplifier," *Optics Letters*, vol. 18, no. 17, pp. 1420-1422, September 1, 1993.
- [8] V.P. Gapontsev, V.V. Formin, I.E. Samartsev, and A. Unt, "25 kW Peak Power, Wide-Tuneable-Repetition_rate and Pulse Duration Eye-Safe MOPFA Laser," *Summaries of Papers of the conference on Lasers and Electro-Optics '96*, pp. 209-211, June 2-7, 1996.
- [9] V.P. Gapontsev, N.S. Platonov, M. Vyatkin, M. Meleshkevitch, D. Spinov, and I. Zaitsev, "3W saturation Power polarization Maintaining 1060 nm Ytterbium Fiber Amplifier," *Proceedings of the SPIE*, vol. 3615, pp. 264-268, January 1999.
- [10] J.A. Alvarez-Chavez, H.L. Offerhaus, J. Nilsson, P.W. Turner, W.A. Clarkson, and D.J. Richardson, "High-Energy, High-Power Ytterbium-Doped q-Switched Fiber Laser," *Optics Letters*, vol. 25, no. 1, pp. 37-39, January 1, 2000.
- [11] G.C. Valley and M. Wright, "Modeling Transient Gain Dynamics in a Cladding-Pumped Yb-Doped Fiber Amplifier Pulsed at Low Repetition Rates," *Summaries of papers of the Conference on Lasers and Electro-Optics 2001, Paper CWA-51, CLEO 2001 Conference, Baltimore, Maryland, May 6-11, 2001.*

- [12] E. Kruger, "High-Repitition-Rate Electro-Optic Cavity Dumping," Review of Scientific Instrumentation, vol. 66, no. 2, pp. 961-967, February 1995.
- [13] D.L. Robinson and M.D. Rayman, "Calculations of Laser Cavity Dumping for Optical Communications," The Telecommunications and Data Acquisition Progress Report 42-95, July-September 1988, Jet Propulsion Laboratory, Pasadena, California, pp. 174-179, November 15, 1988.
http://tmo.jpl.nasa.gov/tmo/progress_report/42-95/95Q.PDF
- [14] D.L. Robinson, "A Novel Approach to a PPM-Mdulated Frequency-Doubled Electro-Optic Cavity-Dumped Nd:YAG Laser," The Telecommunications and Data Acquisition Progress Report 42-97, January-March 1989, Jet Propulsion Laboratory, Pasadena, California, pp. 240-247, May 15, 1989.
http://tmo.jpl.nasa.gov/tmo/progress_report/42-97/97Z.PDF
- [15] G.W. Hollerman and G.S. Mercherle, "Optimization of Pulse-Position Modulation Communication when Using a Cavity-Dumped Nd:YAG Laser," Proceedings of SPIE, vol. 2123, pp. 254-263, January 26-28, 1994.
- [16] K. Shaik, "Progress on Ten-Meter Optical Receiver Telescope," Free Space Laser Communication Technologies IV, SPIE vol. 1635, 1635, pp. 109-117, 1992.
- [17] M.J. Britcliffe and D.J. Hoppe, "Main-Reflector Manufacturing Technology for the Deep Space Optical Communications Ground Station," The Telecommunications and Data Acquisition Progress Report 42-145, May 15, 2001, Jet Propulsion Laboratory, Pasadena, California.
- [18] http://aeronet.gsfc.nasa.gov/F_Info/More.html
- [19] Anthony E. Siegman, Lasers, University Science Books, Mill Valley, California, pp 750-758, Section 19.2 "Important Stable Resonator Types," 1986.
- * This subsection (page 4) was adapted from W.T. Roberts' introduction to the paper, "Cavity-Dumped Communication Laser Design" [Reference 2].
- ** The Experiment Plan written here (page 13) is adapted from one written by W.T. Roberts.

Appendix A. Telescope Schematic for 100 in Telescope at Mt. Wilson



Photograph of blueprint and superposition of current optics positions credit to Jeffrey Charles of JPL.

Appendix B. Photograph of 100 in Telescope at Mt. Wilson



Photograph credit to Jeffrey Charles of JPL.

Appendix D. A List of JPL Optical Communications Group Research Topics for Publications Found at:

<http://lasers.jpl.nasa.gov/PAGES/pubs.html>

FLIGHT TECHNOLOGIES R & D

- ATP- Acquisition, Tracking, & Pointing
- OCD- Optical Communications Demonstrations
- Future Deep Space Missions
- Multi-Gigabit/sec Optical Communications Transceiver for Earth Science
- Component & Subsystem Technology Development
- Coherent Communications
- Small Lasercomm Terminals (ACLAIM & SCOPE)

GROUND TECHNOLOGIES R & D

- OCTL- Optical Communications Telescope Laboratory
- Ground Receivers Antenna Definition
- Optical Systems Analysis
- Optical Receivers
- LTES- Laser Testing & Evaluation Station
- Atmospheric Propagation Studies (AVM)
- Ground-to-Space Optical Communications Demonstration (GOPEX, GOLD, CEMERLL)
- Ground-to-Ground Laser Communication Demonstration

Appendix E. Target Stars for Blind Pointing Accuracy Test

Target Star Name	V Magnitude	RA	DEC
Cygnus (HR7763) Ref. Near Zenith	4.81	20:17:54.9	38:02:38
HR7806	4.43	20:24:00.0	32:12:06
HR7852	4.03	20:33:22.8	11:18:55
HR7928	4.43	20:43:37.3	15:05:14
HR8414	2.96	22:05:57.8	-00:18:10